FERMILAB-PUB-09-066-E

Measurements of differential cross sections of Z/γ^*+jets+X events in $p\bar{p}$ collisions at $\sqrt{s} = 1.96$ TeV

V.M. Abazov[36], B. Abbott[74], M. Abolins[64], B.S. Acharya[29], M. Adams[50], T. Adams[48], E. Aguilo[6], M. Ahsan[58], G.D. Alexeev[36], G. Alkhazov[40], A. Alton[64,a], G. Alverson[62], G.A. Alves[2], L.S. Ancu[35], T. Andeen[52], M.S. Anzelc[52], M. Aoki[49], Y. Arnoud[14], M. Arov[59], M. Arthaud[18], A. Askew[48,b], B. Åsman[41], O. Atramentov[48,b], C. Avila[8], J. BackusMayes[81], F. Badaud[13], L. Bagby[49], B. Baldin[49], D.V. Bandurin[58], P. Banerjee[29], S. Banerjee[29], E. Barberis[62], A.-F. Barfuss[15], P. Bargassa[79], P. Baringer[57], J. Barreto[2], J.F. Bartlett[49], U. Bassler[18], D. Bauer[43], S. Beale[6], A. Bean[57], M. Begalli[3], M. Begel[72], C. Belanger-Champagne[41], L. Bellantoni[49], A. Bellavance[49], J.A. Benitez[64], S.B. Beri[27], G. Bernardi[17], R. Bernhard[23], I. Bertram[42], M. Besançon[18], R. Beuselinck[43], V.A. Bezzubov[39], P.C. Bhat[49], V. Bhatnagar[27], G. Blazey[51], S. Blessing[48], K. Bloom[66], A. Boehnlein[49], D. Boline[61], T.A. Bolton[58], E.E. Boos[38], G. Borissov[42], T. Bose[76], A. Brandt[77], R. Brock[64], G. Brooijmans[69], A. Bross[49], D. Brown[19], X.B. Bu[7], N.J. Buchanan[48], D. Buchholz[52], M. Buehler[80], V. Buescher[22], V. Bunichev[38], S. Burdin[42,c], T.H. Burnett[81], C.P. Buszello[43], P. Calfayan[25], B. Calpas[15], S. Calvet[16], J. Cammin[70], M.A. Carrasco-Lizarraga[33], E. Carrera[48], W. Carvalho[3], B.C.K. Casey[49], H. Castilla-Valdez[33], S. Chakrabarti[71], D. Chakraborty[51], K.M. Chan[54], A. Chandra[47], E. Cheu[45], D.K. Cho[61], S. Choi[32], B. Choudhary[28], L. Christofek[76], T. Christoudias[43], S. Cihangir[49], D. Claes[66], J. Clutter[57], M. Cooke[49], W.E. Cooper[49], M. Corcoran[79], F. Couderc[18], M.-C. Cousinou[15], S. Crépé-Renaudin[14], V. Cuplov[58], D. Cutts[76], M. Ćwiok[30], A. Das[45], G. Davies[43], K. De[77], S.J. de Jong[35], E. De La Cruz-Burelo[33], K. DeVaughan[66], F. Déliot[18], M. Demarteau[49], R. Demina[70], D. Denisov[49], S.P. Denisov[39], S. Desai[49], H.T. Diehl[49], M. Diesburg[49], A. Dominguez[66], T. Dorland[81], A. Dubey[28], L.V. Dudko[38], L. Duflot[16], D. Duggan[48], A. Duperrin[15], S. Dutt[27], A. Dyshkant[51], M. Eads[66], D. Edmunds[64], J. Ellison[47], V.D. Elvira[49], Y. Enari[76], S. Eno[60], P. Ermolov[38,‡], M. Escalier[15], H. Evans[53], A. Evdokimov[72], V.N. Evdokimov[39], A.V. Ferapontov[58], T. Ferbel[61,70], F. Fiedler[24], F. Filthaut[35], W. Fisher[49], H.E. Fisk[49], M. Fortner[51], H. Fox[42], S. Fu[49], S. Fuess[49], T. Gadfort[69], C.F. Galea[35], A. Garcia-Bellido[70], V. Gavrilov[37], P. Gay[13], W. Geist[19], W. Geng[15,64], C.E. Gerber[50], Y. Gershtein[48,b], D. Gillberg[6], G. Ginther[70], B. Gómez[8], A. Goussiou[81], P.D. Grannis[71], S. Greder[19], H. Greenlee[49], Z.D. Greenwood[59], E.M. Gregores[4], G. Grenier[20], Ph. Gris[13], J.-F. Grivaz[16], A. Grohsjean[25], S. Grünendahl[49], M.W. Grünewald[30], F. Guo[71], J. Guo[71], G. Gutierrez[49], P. Gutierrez[74], A. Haas[69], N.J. Hadley[60], P. Haefner[25], S. Hagopian[48], J. Haley[67], I. Hall[64], R.E. Hall[46], L. Han[7], K. Harder[44], A. Harel[70], J.M. Hauptman[56], J. Hays[43], T. Hebbeker[21], D. Hedin[51], J.G. Hegeman[34], A.P. Heinson[47], U. Heintz[61], C. Hensel[22,d], K. Herner[63], G. Hesketh[62], M.D. Hildreth[54], R. Hirosky[80], T. Hoang[48], J.D. Hobbs[71], B. Hoeneisen[12], M. Hohlfeld[22], S. Hossain[74], P. Houben[34], Y. Hu[71], Z. Hubacek[10], N. Huske[17], V. Hynek[10], I. Iashvili[68], R. Illingworth[49], A.S. Ito[49], S. Jabeen[61], M. Jaffré[16], S. Jain[74], K. Jakobs[23], D. Jamin[15], C. Jarvis[60], R. Jesik[43], K. Johns[45], C. Johnson[69], M. Johnson[49], D. Johnston[66], A. Jonckheere[49], P. Jonsson[43], A. Juste[49], E. Kajfasz[15], D. Karmanov[38], P.A. Kasper[49], I. Katsanos[66], V. Kaushik[77], R. Kehoe[78], S. Kermiche[15], N. Khalatyan[49], A. Khanov[75], A. Kharchilava[68], Y.N. Kharzheev[36], D. Khatidze[69], T.J. Kim[31], M.H. Kirby[52], M. Kirsch[21], B. Klima[49], J.M. Kohli[27], J.-P. Konrath[23], A.V. Kozelov[39], J. Kraus[64], T. Kuhl[24], A. Kumar[68], A. Kupco[11], T. Kurča[20], V.A. Kuzmin[38], J. Kvita[9], F. Lacroix[13], D. Lam[54], S. Lammers[53], G. Landsberg[76], P. Lebrun[20], W.M. Lee[49], A. Leflat[38], J. Lellouch[17], J. Li[77,‡], L. Li[47], Q.Z. Li[49], S.M. Lietti[5], J.K. Lim[31], D. Lincoln[49], J. Linnemann[64], V.V. Lipaev[39], R. Lipton[49], Y. Liu[7], Z. Liu[6], A. Lobodenko[40], M. Lokajicek[11], P. Love[42], H.J. Lubatti[81], R. Luna-Garcia[33,e], A.L. Lyon[49], A.K.A. Maciel[2], D. Mackin[79], P. Mättig[26], A. Magerkurth[63], P.K. Mal[81], H.B. Malbouisson[3], S. Malik[66], V.L. Malyshev[36], Y. Maravin[58], B. Martin[14], R. McCarthy[71], C.L. McGivern[57], M.M. Meijer[35], A. Melnitchouk[65], L. Mendoza[8], P.G. Mercadante[5], M. Merkin[38], K.W. Merritt[49], A. Meyer[21], J. Meyer[22,d], J. Mitrevski[69], R.K. Mommsen[44], N.K. Mondal[29], R.W. Moore[6], T. Moulik[57], G.S. Muanza[15], M. Mulhearn[69], O. Mundal[22], L. Mundim[3], E. Nagy[15], M. Naimuddin[49], M. Narain[76], H.A. Neal[63], J.P. Negret[8], P. Neustroev[40], H. Nilsen[23], H. Nogima[3], S.F. Novaes[5], T. Nunnemann[25], D.C. O'Neil[6], G. Obrant[40], C. Ochando[16], D. Onoprienko[58], J. Orduna[33], N. Oshima[49], N. Osman[43], J. Osta[54], R. Otec[10], G.J. Otero y Garzón[1], M. Owen[44], M. Padilla[47], P. Padley[79], M. Pangilinan[76], N. Parashar[55], S.-J. Park[22,d], S.K. Park[31], J. Parsons[69], R. Partridge[76], N. Parua[53], A. Patwa[72], G. Pawloski[79], B. Penning[23], M. Perfilov[38], K. Peters[44], Y. Peters[44], P. Pétroff[16], R. Piegaia[1], J. Piper[64], M.-A. Pleier[22], P.L.M. Podesta-Lerma[33,f], V.M. Podstavkov[49], Y. Pogorelov[54], M.-E. Pol[2], P. Polozov[37], A.V. Popov[39],

C. Potter[6], W.L. Prado da Silva[3], S. Protopopescu[72], J. Qian[63], A. Quadt[22,d], B. Quinn[65], A. Rakitine[42], M.S. Rangel[16], K. Ranjan[28], P.N. Ratoff[42], P. Renkel[78], P. Rich[44], M. Rijssenbeek[71], I. Ripp-Baudot[19], F. Rizatdinova[75], S. Robinson[43], R.F. Rodrigues[3], M. Rominsky[74], C. Royon[18], P. Rubinov[49], R. Ruchti[54], G. Safronov[37], G. Sajot[14], A. Sánchez-Hernández[33], M.P. Sanders[17], B. Sanghi[49], G. Savage[49], L. Sawyer[59], T. Scanlon[43], D. Schaile[25], R.D. Schamberger[71], Y. Scheglov[40], H. Schellman[52], T. Schliephake[26], S. Schlobohm[81], C. Schwanenberger[44], R. Schwienhorst[64], J. Sekaric[48], H. Severini[74], E. Shabalina[50], M. Shamim[58], V. Shary[18], A.A. Shchukin[39], R.K. Shivpuri[28], V. Siccardi[19], V. Simak[10], V. Sirotenko[49], P. Skubic[74], P. Slattery[70], D. Smirnov[54], G.R. Snow[66], J. Snow[73], S. Snyder[72], S. Söldner-Rembold[44], L. Sonnenschein[21], A. Sopczak[42], M. Sosebee[77], K. Soustruznik[9], B. Spurlock[77], J. Stark[14], V. Stolin[37], D.A. Stoyanova[39], J. Strandberg[63], S. Strandberg[41], M.A. Strang[68], E. Strauss[71], M. Strauss[74], R. Ströhmer[25], D. Strom[52], L. Stutte[49], S. Sumowidagdo[48], P. Svoisky[35], M. Takahashi[44], A. Tanasijczuk[1], W. Taylor[6], B. Tiller[25], F. Tissandier[13], M. Titov[18], V.V. Tokmenin[36], I. Torchiani[23], D. Tsybychev[71], B. Tuchming[18], C. Tully[67], P.M. Tuts[69], R. Unalan[64], L. Uvarov[40], S. Uvarov[40], S. Uzunyan[51], B. Vachon[6], P.J. van den Berg[34], R. Van Kooten[53], W.M. van Leeuwen[34], N. Varelas[50], E.W. Varnes[45], I.A. Vasilyev[39], P. Verdier[20], L.S. Vertogradov[36], M. Verzocchi[49], D. Vilanova[18], P. Vint[43], P. Vokac[10], M. Voutilainen[66,g], R. Wagner[67], H.D. Wahl[48], M.H.L.S. Wang[49], J. Warchol[54], G. Watts[81], M. Wayne[54], G. Weber[24], M. Weber[49,h], L. Welty-Rieger[53], A. Wenger[23,i], M. Wetstein[60], A. White[77], D. Wicke[26], M.R.J. Williams[42], G.W. Wilson[57], S.J. Wimpenny[47], M. Wobisch[59], D.R. Wood[62], T.R. Wyatt[44], Y. Xie[76], C. Xu[63], S. Yacoob[52], R. Yamada[49], W.-C. Yang[44], T. Yasuda[49], Y.A. Yatsunenko[36], Z. Ye[49], H. Yin[7], K. Yip[72], H.D. Yoo[76], S.W. Youn[52], J. Yu[77], C. Zeitnitz[26], S. Zelitch[80], T. Zhao[81], B. Zhou[63], J. Zhu[71], M. Zielinski[70], D. Zieminska[53], L. Zivkovic[69], V. Zutshi[51], and E.G. Zverev[38]

(The DØ Collaboration)

[1] *Universidad de Buenos Aires, Buenos Aires, Argentina*
[2] *LAFEX, Centro Brasileiro de Pesquisas Físicas, Rio de Janeiro, Brazil*
[3] *Universidade do Estado do Rio de Janeiro, Rio de Janeiro, Brazil*
[4] *Universidade Federal do ABC, Santo André, Brazil*
[5] *Instituto de Física Teórica, Universidade Estadual Paulista, São Paulo, Brazil*
[6] *University of Alberta, Edmonton, Alberta, Canada; Simon Fraser University, Burnaby, British Columbia, Canada; York University, Toronto, Ontario, Canada and McGill University, Montreal, Quebec, Canada*
[7] *University of Science and Technology of China, Hefei, People's Republic of China*
[8] *Universidad de los Andes, Bogotá, Colombia*
[9] *Center for Particle Physics, Charles University, Faculty of Mathematics and Physics, Prague, Czech Republic*
[10] *Czech Technical University in Prague, Prague, Czech Republic*
[11] *Center for Particle Physics, Institute of Physics, Academy of Sciences of the Czech Republic, Prague, Czech Republic*
[12] *Universidad San Francisco de Quito, Quito, Ecuador*
[13] *LPC, Université Blaise Pascal, CNRS/IN2P3, Clermont, France*
[14] *LPSC, Université Joseph Fourier Grenoble 1, CNRS/IN2P3, Institut National Polytechnique de Grenoble, Grenoble, France*
[15] *CPPM, Aix-Marseille Université, CNRS/IN2P3, Marseille, France*
[16] *LAL, Université Paris-Sud, IN2P3/CNRS, Orsay, France*
[17] *LPNHE, IN2P3/CNRS, Universités Paris VI and VII, Paris, France*
[18] *CEA, Irfu, SPP, Saclay, France*
[19] *IPHC, Université de Strasbourg, CNRS/IN2P3, Strasbourg, France*
[20] *IPNL, Université Lyon 1, CNRS/IN2P3, Villeurbanne, France and Université de Lyon, Lyon, France*
[21] *III. Physikalisches Institut A, RWTH Aachen University, Aachen, Germany*
[22] *Physikalisches Institut, Universität Bonn, Bonn, Germany*
[23] *Physikalisches Institut, Universität Freiburg, Freiburg, Germany*
[24] *Institut für Physik, Universität Mainz, Mainz, Germany*
[25] *Ludwig-Maximilians-Universität München, München, Germany*
[26] *Fachbereich Physik, University of Wuppertal, Wuppertal, Germany*
[27] *Panjab University, Chandigarh, India*
[28] *Delhi University, Delhi, India*
[29] *Tata Institute of Fundamental Research, Mumbai, India*
[30] *University College Dublin, Dublin, Ireland*
[31] *Korea Detector Laboratory, Korea University, Seoul, Korea*
[32] *SungKyunKwan University, Suwon, Korea*

[33] *CINVESTAV, Mexico City, Mexico*
[34] *FOM-Institute NIKHEF and University of Amsterdam/NIKHEF, Amsterdam, The Netherlands*
[35] *Radboud University Nijmegen/NIKHEF, Nijmegen, The Netherlands*
[36] *Joint Institute for Nuclear Research, Dubna, Russia*
[37] *Institute for Theoretical and Experimental Physics, Moscow, Russia*
[38] *Moscow State University, Moscow, Russia*
[39] *Institute for High Energy Physics, Protvino, Russia*
[40] *Petersburg Nuclear Physics Institute, St. Petersburg, Russia*
[41] *Stockholm University, Stockholm, Sweden, and Uppsala University, Uppsala, Sweden*
[42] *Lancaster University, Lancaster, United Kingdom*
[43] *Imperial College, London, United Kingdom*
[44] *University of Manchester, Manchester, United Kingdom*
[45] *University of Arizona, Tucson, Arizona 85721, USA*
[46] *California State University, Fresno, California 93740, USA*
[47] *University of California, Riverside, California 92521, USA*
[48] *Florida State University, Tallahassee, Florida 32306, USA*
[49] *Fermi National Accelerator Laboratory, Batavia, Illinois 60510, USA*
[50] *University of Illinois at Chicago, Chicago, Illinois 60607, USA*
[51] *Northern Illinois University, DeKalb, Illinois 60115, USA*
[52] *Northwestern University, Evanston, Illinois 60208, USA*
[53] *Indiana University, Bloomington, Indiana 47405, USA*
[54] *University of Notre Dame, Notre Dame, Indiana 46556, USA*
[55] *Purdue University Calumet, Hammond, Indiana 46323, USA*
[56] *Iowa State University, Ames, Iowa 50011, USA*
[57] *University of Kansas, Lawrence, Kansas 66045, USA*
[58] *Kansas State University, Manhattan, Kansas 66506, USA*
[59] *Louisiana Tech University, Ruston, Louisiana 71272, USA*
[60] *University of Maryland, College Park, Maryland 20742, USA*
[61] *Boston University, Boston, Massachusetts 02215, USA*
[62] *Northeastern University, Boston, Massachusetts 02115, USA*
[63] *University of Michigan, Ann Arbor, Michigan 48109, USA*
[64] *Michigan State University, East Lansing, Michigan 48824, USA*
[65] *University of Mississippi, University, Mississippi 38677, USA*
[66] *University of Nebraska, Lincoln, Nebraska 68588, USA*
[67] *Princeton University, Princeton, New Jersey 08544, USA*
[68] *State University of New York, Buffalo, New York 14260, USA*
[69] *Columbia University, New York, New York 10027, USA*
[70] *University of Rochester, Rochester, New York 14627, USA*
[71] *State University of New York, Stony Brook, New York 11794, USA*
[72] *Brookhaven National Laboratory, Upton, New York 11973, USA*
[73] *Langston University, Langston, Oklahoma 73050, USA*
[74] *University of Oklahoma, Norman, Oklahoma 73019, USA*
[75] *Oklahoma State University, Stillwater, Oklahoma 74078, USA*
[76] *Brown University, Providence, Rhode Island 02912, USA*
[77] *University of Texas, Arlington, Texas 76019, USA*
[78] *Southern Methodist University, Dallas, Texas 75275, USA*
[79] *Rice University, Houston, Texas 77005, USA*
[80] *University of Virginia, Charlottesville, Virginia 22901, USA and*
[81] *University of Washington, Seattle, Washington 98195, USA*

(Dated: March 10, 2009)

We present cross section measurements for Z/γ^*+jets+X production, differential in the transverse momenta of the three leading jets. The data sample was collected with the D0 detector at the Fermilab Tevatron $p\bar{p}$ collider at a center-of-mass energy of 1.96 TeV and corresponds to an integrated luminosity of 1 fb^{-1}. Leading and next-to-leading order perturbative QCD predictions are compared with the measurements, and agreement is found within the theoretical and experimental uncertainties. We also make comparisons with the predictions of four event generators. Two parton-shower-based generators show significant shape and normalization differences with respect to the data. In contrast, two generators combining tree-level matrix elements with a parton shower give a reasonable description of the the shapes observed in data, but the predicted normalizations show significant differences with respect to the data, reflecting large scale uncertainties. For specific choices of scales, the normalizations for either generator can be made to agree with the measurements.

PACS numbers: 12.38.Qk, 13.85.Qk, 13.87.-a

The production of jets in association with vector bosons (V+jets) in hadron collisions is an important process in quantum chromodynamics (QCD) [1] and is a significant source of background for many standard model measurements (e.g., $t\bar{t}$ production) and in searches for new phenomena (e.g., supersymmetry). Such measurements at the Fermilab Tevatron collider and the CERN Large Hadron Collider (LHC) rely on accurate descriptions of V+jets production by particle-level event generators. These models require validation with measurements of the properties of the V+jets system, especially as a function of jet multiplicity.

In this Letter, we present new precision measurements of differential cross sections for the production of Z/γ^*+jets+X in $p\bar{p}$ collisions at a center-of-mass energy of 1.96 TeV. Cross sections are presented in bins of the transverse momentum (p_T) of the $N^{\rm th}$ jet in events containing at least $N = 1$, 2, or 3 jets and are normalized to the measured inclusive Z/γ^* cross section to reduce uncertainties. The N jets are ordered in terms of decreasing p_T, and the Z/γ^* is selected via its decay into an electron-positron pair. The data set corresponds to an integrated luminosity of 1.04 ± 0.06 fb^{-1} [2].

Previous Z/γ^*+jets measurements have focused primarily on measuring the jet multiplicities for up to three [3] and four [4] jets. In addition, differential distributions have been presented for the highest-p_T (leading) jet [5] and for the two leading jets [3]. In this Letter, we extend the measurements of differential distributions by including the third leading jet, and by including a larger $p_T^{\rm jet}$ range. A major focus of the Letter is a comparison of the differential p_T distributions to leading order (LO) and next-to-leading (NLO) perturbative QCD (pQCD) predictions from MCFM [6], as well as to results from several commonly-used event generators. In particular, we have investigated to what extent the differential p_T distributions for the higher jet multiplicities can be described by parton-shower-based event generators like PYTHIA [7] and HERWIG [8], and how they compare to event generator predictions where matrix element and parton shower merging procedures are adopted, as in ALPGEN+PYTHIA [9] and SHERPA [10]. For each prediction, the renormalization and factorization scale uncertainties are evaluated, and the choices of scales are modified to achieve an improved description of the measurements. The presented studies are of vital importance to understand the predictive power of the various event generator models for V+jets processes at both the Tevatron and the LHC.

The data set was recorded using the D0 Run II detector, which is described in detail elsewhere [11]. Here we give a brief overview of the most relevant components for this analysis. The trajectory of charged particles are reconstructed using a silicon vertex tracker and a scintillating fiber tracker located inside a superconducting solenoidal coil that provides a magnetic field of approximately 2 T. The tracking volume is surrounded by a liquid-argon and uranium calorimeter, divided into electromagnetic and hadronic sections with a granularity of $\Delta\eta \times \Delta\phi = 0.1 \times 0.1$, where η is the pseudorapidity [12] and ϕ is the azimuthal angle. The third layer of the electromagnetic calorimeter has a finer granularity of $\Delta\eta \times \Delta\phi = 0.05 \times 0.05$. The calorimeter consists of three sections, each housed in a separate cryostat, with a central section covering $|\eta| \leq 1.1$ and two end calorimeters extending the coverage to $|\eta| \approx 4.2$. Scintillators between the cryostats sample shower energy for $1.1 < |\eta| < 1.4$.

Electrons are identified based on their characteristic energy deposition signature in the calorimeter, including the transverse and longitudinal shower profiles. In addition, a reconstructed track must point to the energy deposit in the calorimeter, and the momentum of the track and the calorimeter energy must be consistent. Rejection against background from photons and jets is achieved with a likelihood discriminant which uses calorimeter and tracking information [13].

Calorimeter jets are reconstructed using the D0 Run II iterative seed-based cone jet algorithm [14], using a splitting/merging fraction of 0.5 and a cone radius $\mathcal{R} = \sqrt{(\Delta y)^2 + (\Delta\phi)^2} = 0.5$, with y being the rapidity [15]. The input objects are clusters of energy deposited in the calorimeter. Rejection of jets arising from electronic noise in the calorimeter is achieved by using quality and jet shape cuts. The reconstructed jets are corrected for the calorimeter response, instrumental out-of-cone showering effects, and additional energy from multiple $p\bar{p}$ interactions and previous beam crossings. These corrections were derived by exploiting the p_T balance in γ+jet and dijet events. The measurements are performed for jets with $p_T > 20$ GeV and $|\eta| < 2.5$.

Events were required to pass single or dielectron trigger requirements, and to contain two electron candidates with opposite sign electric charge, $p_T > 25$ GeV, $|\eta| < 1.1$ or $1.5 < |\eta| < 2.5$, and a dielectron mass (M_{ee}) satisfying $65 < M_{ee} < 115$ GeV. A total of 65,759 events pass the selection before background subtraction. Of these, 8,452/1,233/167 events have 1/2/3 jets or more, with $p_T^{\rm jet}$ above 20 GeV. The efficiency for the trigger requirements to be satisfied by $Z/\gamma^*(\rightarrow e^+e^-)$ events which fulfill the other selection criteria was found to be $\sim 100\%$, independent of the number of jets in the event.

Backgrounds arising from events which contain two real electrons (e.g., WW, $t\bar{t}$, and $Z/\gamma^*(\rightarrow \tau^+\tau^-)$) were estimated using event samples generated with PYTHIA v6.323, with the underlying event model configured using Tune A [16]. The events were passed through a GEANT-based [17] simulation of the detector response, and each event sample was normalized to higher-order theoretical predictions [6, 18]. The sum of all backgrounds containing two real electrons was estimated to be below 6% in all measurement bins and has been subtracted from the measured data. By studying a sample of same-charge dielectron events, backgrounds arising from events with

one or more mis-reconstructed electrons (e.g., W+jets or multijet events) were found to be below 1% in the inclusive $Z/\gamma^*(\rightarrow e^+e^-)$ sample. For the signal samples containing at least 1, 2, or 3 jets, no statistically significant contribution from W+jets or multijet events was observed. For W+jets, this was confirmed independently by using an event sample generated with PYTHIA, yielding a contribution to the signal samples at the 0.1% level.

The corrections of the reconstructed $p_T^{\rm jet}$ spectra to the particle level [19] were determined using an event sample generated with ALPGEN v2.05 + PYTHIA v6.325 using Tune A. The events were passed through a GEANT-based simulation of the detector response. The simulated events were overlaid with data events from random bunch crossings to reproduce the effects of detector noise and additional $p\bar{p}$ interactions. Particle-level jets were defined through the D0 Run II iterative seed-based cone jet algorithm with $\mathcal{R} = 0.5$ using a splitting/merging fraction of 0.5 and were required to satisfy $|y| < 2.5$. The input objects were all stable particles except the two electrons defining the dielectron system and any photons in a cone of $\mathcal{R} = 0.2$ around the two electrons. The latter requirement excludes most photons associated with the Z/γ^* decays, described in the simulation as QED final-state radiation.

In the simulated sample, the ratio of the reconstructed $p_T^{\rm jet}$ spectrum to the particle level spectrum defines the product of the efficiency of the detector ($\epsilon_{\rm sim}$) and its geometrical acceptance ($A_{\rm sim}$). The product $(\epsilon \times A)$ also includes the impact of the detector resolution on the reconstructed spectrum. To achieve agreement between $(\epsilon \times A)_{\rm sim}$ and the corresponding quantity in data, $(\epsilon \times A)_{\rm data}$, the simulated event sample was modified in two steps. First, the simulated event sample was corrected so that its object identification efficiencies, energy scales, and energy resolutions correspond to those measured in data. Next, the shapes of the $p_T^{\rm jet}$ spectra in the simulated sample were reweighted at the particle level so that agreement with data was obtained at the reconstructed level. These two steps are explained in more detail below.

The single electron identification efficiency was measured in data for inclusive $Z/\gamma^*(\rightarrow e^+e^-)+X$ events [20], giving an efficiency, including statistical uncertainty, of $\epsilon^e_{\rm data} = 0.77 \pm 0.01$. The electron identification efficiency in the simulated sample, $\epsilon^e_{\rm sim}$, was found to be $\approx 10\%$ higher than in data. To adjust the simulation to correspond to data, each reconstructed electron candidate in the simulated sample was rejected with a probability given by $\epsilon^e_{\rm data}/\ \epsilon^e_{\rm sim}$. The electron efficiencies were binned in η_e and ϕ_e. As a cross check, the analysis was also performed using electron efficiencies binned in η_e and $p_{T,e}$, resulting in changes of less than 1% in the final measurements. The same correction procedure was applied for the identification efficiency for jets, which was found to be $\epsilon^{\rm jet}_{\rm data} = 0.98 \pm 0.02$ in data.

The electron identification efficiency depends on the number of jets in an event and on their kinematics. Electron candidates with a nearby jet are less likely to pass the electron identification criteria. To determine if the correlation between the electron efficiencies and the jet activity is correctly described by the simulation, two sets of comparisons were performed. First, the minimal $\Delta\mathcal{R}$ separation between each electron and all jets in N-jet events ($N = 0, 1, 2, 3$) in the simulated sample were compared with data. Second, the amount of soft QCD radiation not clustered into jets was studied using tracks which were not associated with any reconstructed electron or jet. The multiplicity and p_T sum of all such tracks in N-jet events ($N = 1, 2, 3$), relative to those in 0-jet events, were compared between simulation and data. For both sets of comparisons, reasonable agreement was found. The total uncertainty due to differences between the simulation and the data in the dependence of the electron identification efficiency on jet activity was estimated to be below 2% for all cross section measurements.

Jet energy scale (JES) corrections were derived using γ+jet and dijet events, assuring that the reconstructed $p_T^{\rm jet}$ in γ+jet events on average is equal to the particle-level $p_T^{\rm jet}$. The difference in calorimeter response between quark- and gluon-initiated jets introduces a dependence of the JES on the physics process. As a result, the JES corrections derived using γ+jet events do not guarantee a correct JES when applied to Z/γ^*+jet events. However, the correction of data to the particle level depends only on data and simulation having a common JES. The factor $(\epsilon \times A)$ accounts for any differences between this common JES and the correct JES since particle-level jets in the simulated sample by definition have the proper energy scale. The p_T balance in Z/γ^*+jet events was used to adjust the JES in simulation to be equal to the JES in data. This correction varies from $\sim 5\%$ below 40 GeV to $\sim 0\%$ above 80 GeV.

The jet energy resolution (JER) in data and simulated events was determined using Z/γ^*+jet events, and the reconstructed jet energies in the simulated sample were corrected to account for any differences. The JER distorts the steeply falling jet p_T spectra, resulting in a net migration towards higher values of $p_T^{\rm jet}$. This leads to the reconstructed $p_T^{\rm jet}$ spectra being (5–15)% higher than they would have been for a detector with perfect jet energy resolution. The factor $(\epsilon \times A)$ accounts for this effect, and the measurements are fully corrected for the JER.

After adjusting the simulated detector performance to the real detector performance, we tuned the $p_T^{\rm jet}$ spectra in the simulation to those observed in data. For the measurement of each observable, the simulated event sample was reweighted as a function of that observable at the particle level to ensure agreement of the distribution of the observable at the reconstructed level. After the reweighting, $(\epsilon \times A)_{\rm sim}$ is equal to $(\epsilon \times A)_{\rm data}$ within the

uncertainties of the corrections applied to the simulated sample. The particle level spectra in data equal the reconstructed spectra in data divided by $(\epsilon \times A)_{\rm sim}$. The total efficiency for reconstructing a $Z/\gamma^*(\rightarrow e^+e^-) + N$-jets+$X$ event varies with $p_T^{\rm jet}$ and is in the range 0.5–0.7 for $N = 1$ and 0.4–0.5 for $N = 2, 3$.

For events containing more than one jet, the $N^{\rm th}$ jet at the particle level might not be equal to the $N^{\rm th}$ jet at the reconstructed level. This can occur for events containing two jets with similar values of $p_T^{\rm jet}$. The impact of this effect is part of $(\epsilon \times A)$ as defined above, and it is correctly taken into account if the JER is identical for simulation and data, and if two jets have similar $p_T^{\rm jet}$ values equally often in simulation and in data. The former is assured by the JER corrections applied to the simulated event sample, as described above. To test if the latter is satisfied, the ratios of the reconstructed p_T-spectrum of the $N^{\rm th}$ jet to the spectra of the $(N-1)^{\rm th}$ jet and the $(N+1)^{\rm th}$ jet in the simulated event sample was compared with those observed in data. Agreement was observed within statistical uncertainties.

The final measurements are presented with two different particle-level selections in the mass range $65 < M_{ee} < 115$ GeV: first without any further selections on the electrons (selection *a*) and secondly requiring $p_T^e > 25$ GeV and $|y^e| < 1.1$ or $1.5 < |y^e| < 2.5$ (selection *b*). Selection *b* corresponds to the kinematic range which is measured in data. Selection *a* includes an extrapolation to the full range of lepton kinematics in order to simplify direct comparisons with other measurements. For each particle-level electron selection, the $p_T^{\rm jet}$ spectra were normalized to the inclusive $Z/\gamma^*(\rightarrow e^+e^-) + X$ cross section measured with the same particle-level selection. The extrapolation from selection *b* to selection *a* increases the normalized differential cross section for the leading jet by $\approx 10\%$ below 100 GeV and decreases it by $\approx 25\%$ above 200 GeV. For the second (third) jet, the extrapolation changes the observable by less than 10% (2%).

The main systematic uncertainty of the measurements arise from the correction of the JES in the simulated event sample to correspond to the JES of the data sample. This source of uncertainty contributes (50–80)% of the total systematic uncertainty of the measurements. Additional uncertainties arise from the reweighting function applied to the simulated event sample at the particle level to ensure agreement with data at the reconstructed level, from the correction of the jet energy resolution and of the jet and electron identification efficiencies in the simulated event sample, and from the extrapolation from selection *b* to selection *a*. The individual systematic uncertainties were added in quadrature to obtain the total systematic uncertainty. Presenting the measurements as ratios to the inclusive $Z/\gamma^*(\rightarrow e^+e^-) + X$ cross section cancels the dependence on the uncertainty in the integrated luminosity of the data set. Additionally, most of the dependence on the uncertainties in the electron trigger and identification efficiencies also cancels.

The choice of binning for the measurements was guided by the finite JER, which causes events to contribute to different bins at the particle and reconstruction levels. The purity of a bin is defined as the fraction of the simulated events which are reconstructed in the same bin in which they were generated at the particle level. The widths of the measurement bins were chosen so that each bin has a purity of about 60%.

The measurements presented above are compared with the predictions of several different theoretical models. For each model, the predicted jet p_T spectra are normalized to the predicted inclusive $Z/\gamma^*(\rightarrow e^+e^-) + X$ cross section. All predictions were generated using the CTEQ 6.1M [21] parton density functions (PDFs) and the two-loop formula for the evolution of the strong coupling constant (α_S). For the first and second jets the NLO MCFM predictions have been taken as the reference prediction; for the third jet, the leading-order (LO) MCFM prediction plays this role. The measurements and all theoretical predictions are presented as ratios with respect to the reference prediction.

The fully corrected measurements are summarized in Tables I–III and graphically represented in Figs. 1–3. The data points are shown with statistical uncertainties (inner uncertainty bars) as well as with statistical and systematic uncertainties combined in quadrature (outer bars). Each data point is placed at the p_T value where the theoretical differential cross section is equal to the average cross section within the bin [22].

The first comparison was performed between data and the pQCD predictions from MCFM v5.3 at NLO for the two leading jets, and at LO for the three leading jets. The central predictions were defined using factorization and renormalization scales $\mu_F = \mu_R = \sqrt{M_Z^2 + p_{T,Z}^2}$, with M_Z and $p_{T,Z}$ denoting the mass and transverse momentum of the Z/γ^* boson. The sensitivity of the predicted cross sections to the choice of μ_F and μ_R was tested by varying their values up and down from the nominal value by a factor of two. The MCFM predictions were multiplied by correction factors accounting for multiple parton interactions ($C_{\rm MPI}$) and hadronization ($C_{\rm Had}$) before being compared to the measurements.

The correction factors $C_{\rm MPI}$ and $C_{\rm Had}$ were estimated using inclusive $Z/\gamma^*(\rightarrow e^+e^-)$ event samples generated with PYTHIA v6.416 using Tune QW [23], PYTHIA v6.416 using Tune S0 [24], HERWIG v6.510 + JIMMY v4.31 [25], ALPGEN v2.13 + PYTHIA v6.325 using Tune QW, and SHERPA v1.1.1. The central values quoted in Tables IV–VI correspond to the predictions of PYTHIA Tune QW. The maximal upwards and downwards differences between PYTHIA Tune QW and the other four models are quoted as systematic uncertainties.

Both the NLO and the LO MCFM predictions are in agreement with the measurements within the experimen-

TABLE I: The measurements of $\frac{1}{\sigma_{Z/\gamma^*}} \times \frac{d\sigma}{dp_T}$ for the first jet (p_T ordered) in $Z/\gamma^*(\rightarrow e^+e^-)$ events with one or more jets.

		$p_T^e > 25$ GeV, $\lvert y^e\rvert < 1.1$ or $1.5 < \lvert y^e\rvert < 2.5$, $65 < M_{ee} < 115$ GeV			$65 < M_{ee} < 115$ GeV		
p_T bin [GeV]	Bin center [GeV]	$1/\sigma_{Z/\gamma^*} \times d\sigma/dp_T^{\rm jet}$ [1/GeV]	$\delta_{\rm stat}$ (%)	$\delta_{\rm sys}$ (%)	$1/\sigma_{Z/\gamma^*} \times d\sigma/dp_T^{\rm jet}$ [1/GeV]	$\delta_{\rm stat}$ (%)	$\delta_{\rm sys}$ (%)
20 – 28	23.7	6.81×10^{-3}	1.6	5.9	7.19×10^{-3}	1.6	7.0
28 – 40	33.5	2.99×10^{-3}	2.1	4.0	3.22×10^{-3}	2.1	4.6
40 – 54	46.4	1.23×10^{-3}	3.1	3.3	1.37×10^{-3}	3.1	3.9
54 – 73	62.7	5.04×10^{-4}	4.0	3.3	5.74×10^{-4}	4.0	4.1
73 – 95	83.1	2.03×10^{-4}	5.6	7.6	2.27×10^{-4}	5.6	8.2
95 – 120	106.2	7.29×10^{-5}	8.4	8.4	7.62×10^{-5}	8.4	8.9
120 – 154	135.3	2.64×10^{-5}	12	10	2.54×10^{-5}	12	11
154 – 200	172.9	8.08×10^{-6}	17	14	6.99×10^{-6}	17	14
200 – 300	236.9	7.46×10^{-7}	42	25	5.58×10^{-7}	42	25

TABLE II: The measurements of $\frac{1}{\sigma_{Z/\gamma^*}} \times \frac{d\sigma}{dp_T}$ for the second jet (p_T ordered) in $Z/\gamma^*(\rightarrow e^+e^-)$ events with two or more jets.

		$p_T^e > 25$ GeV, $\lvert y^e\rvert < 1.1$ or $1.5 < \lvert y^e\rvert < 2.5$, $65 < M_{ee} < 115$ GeV			$65 < M_{ee} < 115$ GeV		
p_T bin [GeV]	Bin center [GeV]	$1/\sigma_{Z/\gamma^*} \times d\sigma/dp_T^{\rm jet}$ [1/GeV]	$\delta_{\rm stat}$ (%)	$\delta_{\rm sys}$ (%)	$1/\sigma_{Z/\gamma^*} \times d\sigma/dp_T^{\rm jet}$ [1/GeV]	$\delta_{\rm stat}$ (%)	$\delta_{\rm sys}$ (%)
20 – 28	23.6	1.30×10^{-3}	3.7	10	1.39×10^{-3}	3.7	11
28 – 40	33.3	4.23×10^{-4}	5.7	5.2	4.51×10^{-4}	5.7	6.0
40 – 54	46.2	1.57×10^{-4}	9.1	6.2	1.62×10^{-4}	9.1	6.8
54 – 73	62.3	4.17×10^{-5}	15	8.5	4.20×10^{-5}	15	9.0
73 – 200	112.9	2.96×10^{-6}	22	7.4	2.82×10^{-6}	22	8.0

TABLE III: The measurements of $\frac{1}{\sigma_{Z/\gamma^*}} \times \frac{d\sigma}{dp_T}$ for the third jet (p_T ordered) in $Z/\gamma^*(\rightarrow e^+e^-)$ events with three or more jets.

		$p_T^e > 25$ GeV, $\lvert y^e\rvert < 1.1$ or $1.5 < \lvert y^e\rvert < 2.5$, $65 < M_{ee} < 115$ GeV			$65 < M_{ee} < 115$ GeV		
p_T bin [GeV]	Bin center [GeV]	$1/\sigma_{Z/\gamma^*} \times d\sigma/dp_T^{\rm jet}$ [1/GeV]	$\delta_{\rm stat}$ (%)	$\delta_{\rm sys}$ (%)	$1/\sigma_{Z/\gamma^*} \times d\sigma/dp_T^{\rm jet}$ [1/GeV]	$\delta_{\rm stat}$ (%)	$\delta_{\rm sys}$ (%)
20 – 28	23.6	2.22×10^{-4}	9.1	14	2.33×10^{-4}	9.1	16
28 – 44	34.6	4.40×10^{-5}	17	8.4	4.48×10^{-5}	17	11
44 – 60	50.9	8.67×10^{-6}	42	11	8.60×10^{-6}	42	13

tal and theoretical uncertainties (Figs. 1–3). At NLO, varying the scales up (down) by a factor of two changes the normalized $p_T^{\rm jet}$ spectrum down (up) by factor of ≈1.1 for the leading jet, compared to a factor ≈1.2 for LO. For the second jet, the factors are ≈1.1 (NLO) and ≈1.4 (LO), and for the third ≈1.6 (LO). These numbers illustrate the improved predictive power of the NLO computation as compared with the LO one. The uncertainties of the MCFM predictions due to the PDFs were evaluated using the Hessian method [26]. For the two leading jets, they vary from 5% at low p_T to 10% at high p_T, and for the third jet they are found to be (5–15)%.

Next, we compare the predictions of PYTHIA v6.416 and HERWIG v6.510 + JIMMY v4.31 with the measurements. These event generators describe jets through a parton shower using the approximation that parton emissions are soft or collinear. For the hard $q\bar{q} \rightarrow Z/\gamma^*$ scattering, both generators use $\mu_F = \mu_R = M_Z$. For the parton shower, theoretical arguments favor the choice $\mu_F = \mu_R = p_T^{\rm rel}$, with $p_T^{\rm rel}$ being the relative transverse momentum between the daughter partons in each $1 \rightarrow 2$ parton splitting [27]. This choice of scales is adopted in HERWIG, and in the final-state shower of PYTHIA. For the initial-state shower, PYTHIA uses $\mu_F = \mu_R = a \times p_T^{\rm rel}$, with a being a constant. For PYTHIA using Tune QW, a is taken to be $\sqrt{0.2}$, whereas for PYTHIA using Tune S0, a is set to 1.0. Both HERWIG and PYTHIA reweight the leading parton shower emission to reproduce Z/γ^*+jet LO matrix-element computations [28]. For the leading jet, PYTHIA using Tune QW shows a more steeply falling spectrum than observed in data (Fig. 1). The prediction of HERWIG + JIMMY shows good agreement with

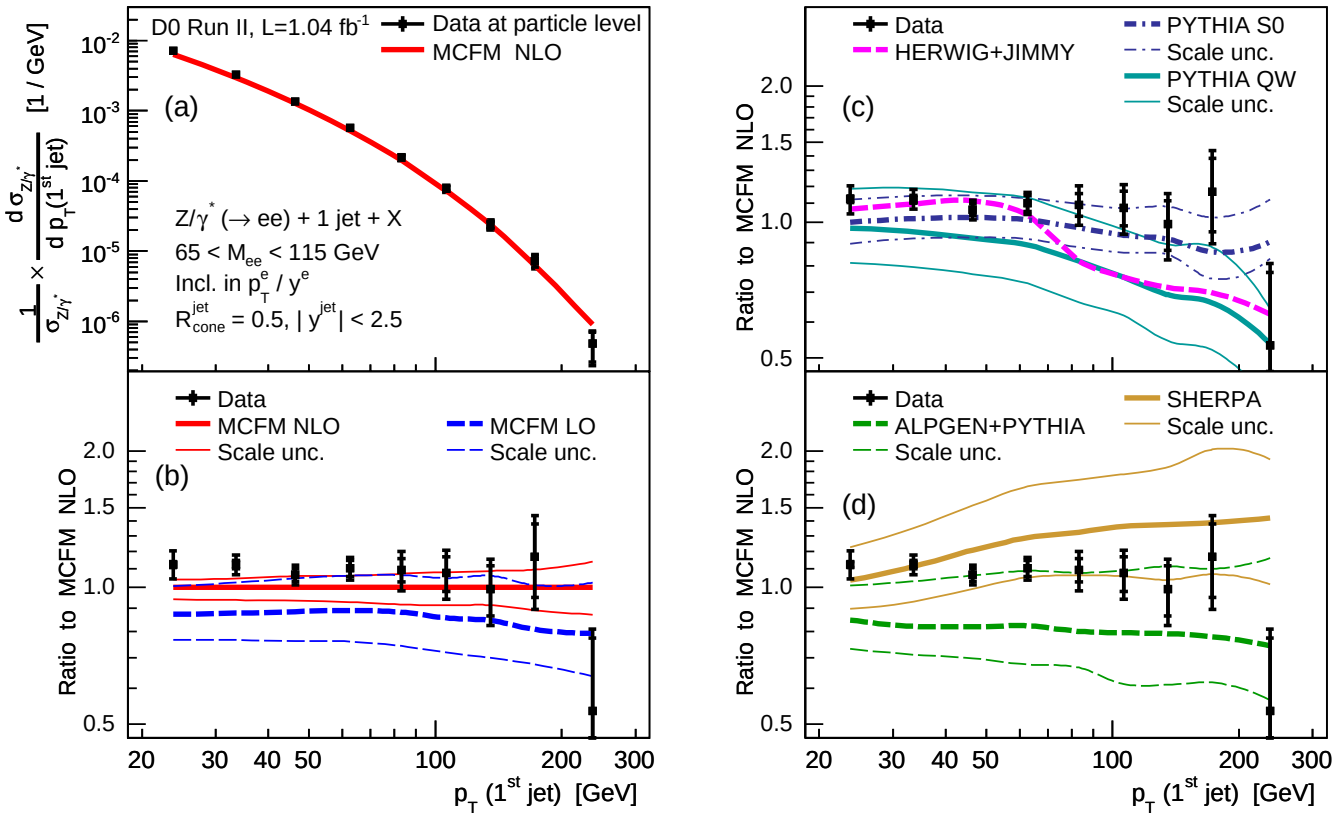

FIG. 1: (a) The measured distribution of $\frac{1}{\sigma_{Z/\gamma^*}} \times \frac{d\sigma}{dp_T(\text{jet})}$ for the leading jet in Z/γ^*+jet+X events, compared to the predictions of MCFM NLO. The ratios of data and theory predictions to MCFM NLO are shown (b) for pQCD predictions corrected to the particle level, (c) for three parton-shower event generator models, and (d) for two event generators matching matrix-elements to a parton shower. The scale uncertainties were evaluated by varying the factorization and renormalization scales by a factor of two.

TABLE IV: Correction factors for multiple parton interactions (C_{MPI}) and hadronization (C_{Had}) for $\frac{1}{\sigma_{Z/\gamma^*}} \times \frac{d\sigma}{dp_T(1^{\text{st}}\text{ jet})}$.

p_T bin [GeV]	$C_{\text{MPI}} \pm (\text{stat}) \pm (\text{sys})$	$C_{\text{Had}} \pm (\text{stat}) \pm (\text{sys})$
20 – 28	$1.08 \pm 0.00^{+0.07}_{-0.04}$	$0.89 \pm 0.00^{+0.04}_{-0.03}$
28 – 40	$1.04 \pm 0.00^{+0.02}_{-0.02}$	$0.90 \pm 0.00^{+0.03}_{-0.01}$
40 – 54	$1.02 \pm 0.00^{+0.01}_{-0.01}$	$0.90 \pm 0.00^{+0.02}_{-0.00}$
54 – 73	$1.02 \pm 0.01^{+0.00}_{-0.02}$	$0.92 \pm 0.01^{+0.01}_{-0.03}$
73 – 95	$1.01 \pm 0.01^{+0.03}_{-0.01}$	$0.93 \pm 0.01^{+0.01}_{-0.02}$
95 – 120	$1.02 \pm 0.02^{+0.00}_{-0.03}$	$0.91 \pm 0.02^{+0.03}_{-0.00}$
120 – 154	$1.04 \pm 0.03^{+0.00}_{-0.07}$	$0.92 \pm 0.02^{+0.05}_{-0.03}$
154 – 200	$1.03 \pm 0.05^{+0.02}_{-0.06}$	$0.91 \pm 0.04^{+0.04}_{-0.06}$
200 – 300	$1.01 \pm 0.09^{+0.04}_{-0.05}$	$0.92 \pm 0.08^{+0.05}_{-0.06}$

TABLE V: Correction factors for multiple parton interactions (C_{MPI}) and hadronization (C_{Had}) for $\frac{1}{\sigma_{Z/\gamma^*}} \times \frac{d\sigma}{dp_T(2^{\text{nd}}\text{ jet})}$.

p_T bin [GeV]	$C_{\text{MPI}} \pm (\text{stat}) \pm (\text{sys})$	$C_{\text{Had}} \pm (\text{stat}) \pm (\text{sys})$
20 – 28	$1.15 \pm 0.01^{+0.06}_{-0.10}$	$0.81 \pm 0.01^{+0.07}_{-0.00}$
28 – 40	$1.10 \pm 0.01^{+0.00}_{-0.07}$	$0.83 \pm 0.01^{+0.05}_{-0.00}$
40 – 54	$1.07 \pm 0.02^{+0.00}_{-0.06}$	$0.85 \pm 0.01^{+0.06}_{-0.00}$
54 – 73	$1.04 \pm 0.03^{+0.00}_{-0.07}$	$0.87 \pm 0.03^{+0.07}_{-0.01}$
73 –200	$1.05 \pm 0.05^{+0.00}_{-0.08}$	$0.83 \pm 0.04^{+0.18}_{-0.00}$

data at low p_T^{jet}, but resembles PYTHIA Tune QW at high p_T^{jet}. The change of slope around $p_T^{\text{jet}} = 50$ GeV can be traced back to the matrix-element correction algorithm in HERWIG [29]. Comparisons to the measurements of the sub-leading jets (Figs. 2–3) show that PYTHIA using Tune QW and HERWIG predict more steeply falling p_T^{jet} spectra than observed in data, in agreement with expectations based on the limited validity of the soft/collinear approximation of the parton shower. A newer PYTHIA model with a p_T-ordered parton shower, using Tune S0, gives a good description of the leading jet, but shows no improvement for the second or third jet. For the two PYTHIA models, samples were generated with μ_F and μ_R being varied up and down from the nominal value by a factor of two. As expected, decreasing μ_F and μ_R increases the predicted amount of events with one or more

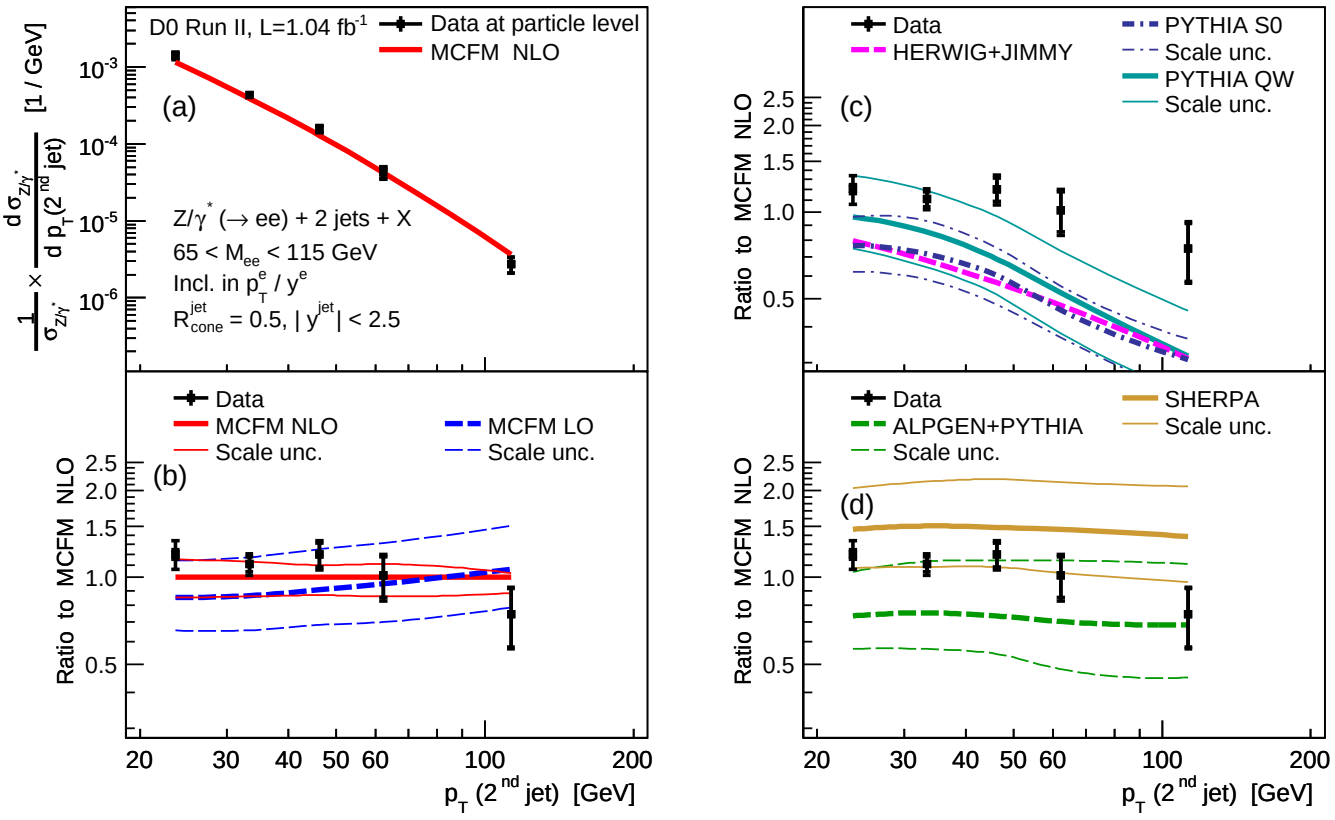

FIG. 2: (a) The measured distribution of $\frac{1}{\sigma_{Z/\gamma^*}} \times \frac{d\sigma}{dp_T(\text{jet})}$ for the second jet in $Z/\gamma^* + 2$ jets+X events, compared to the predictions of MCFM NLO. The ratios of data and theory predictions to MCFM NLO are shown (b) for pQCD predictions corrected to the particle level, (c) for three parton-shower event generator models, and (d) for two event generators matching matrix-elements to a parton shower. The scale uncertainties were evaluated by varying the factorization and renormalization scales by a factor of two.

TABLE VI: Correction factors for multiple parton interactions (C_{MPI}) and hadronization (C_{Had}) for $\frac{1}{\sigma_{Z/\gamma^*}} \times \frac{d\sigma}{dp_T(3^{\text{rd}}\text{ jet})}$.

p_T bin [GeV]	$C_{\text{MPI}} \pm (\text{stat}) \pm (\text{sys})$	$C_{\text{Had}} \pm (\text{stat}) \pm (\text{sys})$
20 – 28	$1.15 \pm 0.02^{+0.00}_{-0.07}$	$0.76 \pm 0.01^{+0.08}_{-0.00}$
28 – 44	$1.10 \pm 0.03^{+0.05}_{-0.04}$	$0.81 \pm 0.03^{+0.05}_{-0.00}$
44 – 60	$1.11 \pm 0.10^{+0.04}_{-0.10}$	$0.74 \pm 0.07^{+0.19}_{-0.00}$

jets. The slopes of the predicted distributions do not change significantly as the scales are varied.

Finally, we show comparisons with the ALPGEN v2.13 + PYTHIA v6.325 and SHERPA v1.1.1 event generators. Both generators combine tree-level matrix elements with parton showers [30–32], thereby utilizing matrix elements also for sub-leading jets. For the central ALPGEN+PYTHIA prediction, the factorization scale is given by $\mu_F = \sqrt{M_Z^2 + p_{T,Z}^2}$, whereas the renormalization scale is defined individually for each parton splitting using the CKKW prescription [30]. For SHERPA, both the factorization and the renormalization scales are given by the CKKW prescription. For all three p_T^{jet} spectra, ALPGEN+PYTHIA predicts lower production rates than observed in data, but the shapes of the spectra are well described. SHERPA predicts a less steeply falling leading p_T^{jet} spectrum than seen in data, leading to disagreements above 40 GeV. For the sub-leading p_T^{jet} spectra, SHERPA predicts higher production rates than observed in data, but the shapes are well described. In agreement with Ref. [31], both ALPGEN+PYTHIA and SHERPA are found to show a sensitivity to the choice of scales which is similar to that of a LO pQCD prediction, reflecting a limited predictive power. For the leading jet at $p_T = 100$ GeV, the prediction of SHERPA with both scales shifted down by a factor of two is about three times higher than the ALPGEN+PYTHIA prediction with both scales shifted up. This reflects both the size of the scale uncertainties and the difference in the central prediction between the two event generators. For ALPGEN+PYTHIA, good and simultaneous agreement with data for all three leading jets is achieved through scaling μ_F and μ_R down by a factor of two from the default values. For SHERPA, an improved description of data is achieved by scaling μ_F

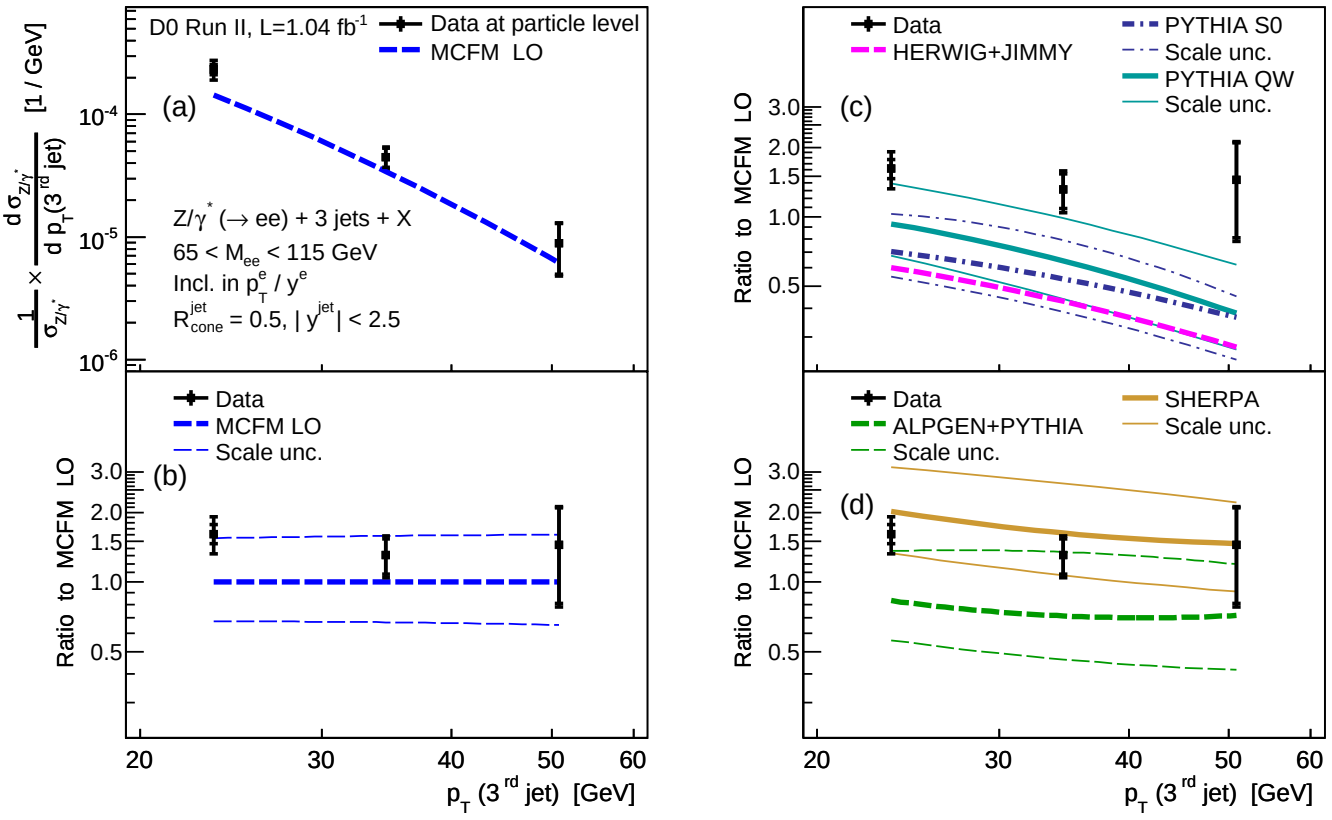

FIG. 3: (a) The measured distribution of $\frac{1}{\sigma_{Z/\gamma^*}} \times \frac{d\sigma}{dp_T(\text{jet})}$ for the third jet in Z/γ^*+3 jets+X events, compared to the predictions of MCFM LO. The ratios of data and theory predictions to MCFM NLO are shown (b) for pQCD predictions corrected to the particle level, (c) for three parton-shower event generator models, and (d) for two event generators matching matrix-elements to a parton shower. The scale uncertainties were evaluated by varying the factorization and renormalization scales by a factor of two.

and μ_R up by factor of two, but remaining disagreements with the measurements are seen for the leading jet below ~ 40 GeV.

In summary, we have presented new measurements of differential cross sections for $Z/\gamma^*(\rightarrow e^+e^-)$+jets+$X$ production in $p\bar{p}$ collisions at a center-of-mass energy of 1.96 TeV using a data sample recorded by the D0 detector corresponding to 1.04 ± 0.06 fb^{-1}. The measurements are binned in the p_T of the N^{th} jet, using events containing at least $N = 1$, 2, or 3 jets, and are normalized to the measured inclusive $Z/\gamma^*(\rightarrow e^+e^-) + X$ cross section. Predictions of MCFM at NLO, corrected to the particle level, are found to be in good agreement with data and have a significantly smaller scale uncertainty than MCFM at LO. The parton-shower based HERWIG and PYTHIA Tune QW event generator models show significant disagreements with data which increase with p_T^{jet} and the number of jets in events. The newer p_T-ordered shower model in PYTHIA gives a good description of the leading jet, but shows no improvement over the old model for the sub-leading jets. The SHERPA and ALPGEN+PYTHIA generators show an improved description of data as compared with the parton-shower-based generators. ALPGEN+PYTHIA gives a good description of the shapes of the p_T^{jet} spectra, while predicting lower production rates than observed in data. SHERPA predicts higher production rates and a less steeply falling p_T^{jet} spectrum for the leading jet than observed in data. For ALPGEN+PYTHIA, the factorization and renormalization scales can be chosen so that a good, simultaneous agreement with data is achieved for all three leading jets. For SHERPA, a similar level of agreement is achieved for the sub-leading jets, but some disagreements remain for the shape of the leading p_T^{jet} spectrum. Since the presented measurements are fully corrected for instrumental effects, they can be used for testing and tuning of present and future event generator models.

We thank the staffs at Fermilab and collaborating institutions, and acknowledge support from the DOE and NSF (USA); CEA and CNRS/IN2P3 (France); FASI, Rosatom and RFBR (Russia); CNPq, FAPERJ, FAPESP and FUNDUNESP (Brazil); DAE and DST (India); Colciencias (Colombia); CONACyT (Mexico); KRF and KOSEF (Korea); CONICET and UBACyT

(Argentina); FOM (The Netherlands); STFC (United Kingdom); MSMT and GACR (Czech Republic); CRC Program, CFI, NSERC and WestGrid Project (Canada); BMBF and DFG (Germany); SFI (Ireland); The Swedish Research Council (Sweden); CAS and CNSF (China); and the Alexander von Humboldt Foundation (Germany).

[a] Visitor from Augustana College, Sioux Falls, SD, USA.
[b] Visitor from Rutgers University, Piscataway, NJ, USA.
[c] Visitor from The University of Liverpool, Liverpool, UK.
[d] Visitor from II. Physikalisches Institut, Georg-August-University, Göttingen, Germany.
[e] Visitor from Centro de Investigacion en Computacion - IPN, Mexico City, Mexico.
[f] Visitor from ECFM, Universidad Autonoma de Sinaloa, Culiacán, Mexico.
[g] Visitor from Helsinki Institute of Physics, Helsinki, Finland.
[h] Visitor from Universität Bern, Bern, Switzerland.
[i] Visitor from Universität Zürich, Zürich, Switzerland.
[‡] Deceased.

[1] D. J. Gross and F. Wilczek, Phys. Rev. D **8**, 3633 (1973).
[2] T. Andeen *et al.*, FERMILAB-TM-2365 (2007).
[3] CDF Collaboration, T. Aaltonen *et al.*, Phys. Rev. Lett. **100**, 102001 (2008).
[4] D0 Collaboration, V. M. Abazov *et al.*, Phys. Lett. B **658**, 112 (2008).
[5] D0 Collaboration, V. M. Abazov *et al.*, Phys. Lett. B **669**, 278 (2008).
[6] J. Campbell and R. K. Ellis, Phys. Rev. D **65**, 113007 (2002).
[7] T. Sjöstrand *et al.*, JHEP **0605**, 026 (2006).
[8] G. Corcella *et al.*, JHEP **0101**, 010 (2001).
[9] M. L. Mangano *et al.*, JHEP **0307**, 001 (2003).
[10] T. Gleisberg *et al.*, JHEP **0402**, 056 (2004).
[11] D0 Collaboration, V. M. Abazov *et al.*, Nucl. Instrum. Methods Phys. Res. A **565**, 463 (2006).
[12] Pseudorapidity is defined as $\eta = -\ln[\tan(\theta/2)]$, with θ being the polar angle measured relative to the proton beam direction.
[13] D0 Collaboration, V. M. Abazov *et al.*, Phys. Rev. D **76**, 092007 (2007).
[14] G. C. Blazey *et al.*, in *Proceedings of the Workshop: QCD and Weak Boson Physics in Run II*, edited by U. Baur, R. K. Ellis, and D. Zeppenfeld, Fermilab-Pub-00/297 (2000).
[15] Rapidity is defined as $y = \ln[(E+p_z)/(E-p_z)]$, where E is the energy and p_z is the momentum along the proton beam direction.
[16] CDF Collaboration, T. Aaltonen *et al.*, Phys. Rev. D **65**, 092002 (2002).
[17] R. Brun and F. Carminati, *CERN Program Library Long Writeup* W5013, 1993 (unpublished).
[18] M. Cacciari *et al.*, JHEP **0404**, 068 (2004).
[19] C. Buttar *et al.*, arXiv:hep-ph/0803.0678 (2008). A detailed discussion is given in Sect. 9.
[20] D0 Collaboration, V. M. Abazov *et al.*, Phys. Rev. D **76**, 012003 (2007).
[21] D. Stump *et al.*, JHEP **0310**, 046 (2003).
[22] G. D. Lafferty and T. R. Wyatt, Nucl. Instrum. Methods Phys. Res. A **355**, 541 (1995).
[23] M. G. Albrow *et al.*, arXiv:hep-ph/0610012 (2006).
[24] T. Sjöstrand and P. Skands, Eur. Phys. J. C **39**, 129 (2005); P. Skands and D. Wicke, Eur. Phys. J. C **52**, 133 (2007).
[25] J. M. Butterworth, J. R. Forshaw and M. H. Seymour, Z. Phys. C **72**, 637 (1996).
[26] J. Pumplin *et al.*, Phys. Rev. D **65**, 014013 (2002).
[27] D. Amati *et al.*, Nucl. Phys. **B173**, 429 (1980).
[28] M. Bengtsson and T. Sjöstrand, Nucl. Phys. **B289**, 810 (1987); M. H. Seymour, Comput. Phys. Comm. **90**, 95 (1995); M. H. Seymour, Nucl. Phys. **B436**, 443 (1995).
[29] M. H. Seymour, private communication.
[30] S. Catani *et al.*, JHEP **0111**, 063 (2001); F. Krauss, JHEP **0208**, 015 (2002); F. Krauss *et al.*, Phys. Rev. D **70**, 114009 (2004).
[31] J. Alwall *et al.*, Eur. Phys. J. C **53**, 473 (2008).
[32] M. L. Mangano *et al.*, JHEP **0701**, 013 (2007).